Dynamics at infinity and the existence of singularly degenerate heteroclinic cycles in the Lorenz system

2009 J. Phys. A: Math. Theor. 42 115101

(http://iopscience.iop.org/1751-8121/42/11/115101)

IOP PUBLISHING JOURNAL OF PHYSICS A: MATHEMATICAL AND THEORETICAL

J. Phys. A: Math. Theor. **42** (2009) 115101 (18pp) doi:10.1088/1751-8113/42/11/115101

Dynamics at infinity and the existence of singularly degenerate heteroclinic cycles in the Lorenz system

Marcelo Messias

Departamento de Matemática, Estatística e Computação, Faculdade de Ciências e Tecnologia, Universidade Estadual Paulista, UNESP, Cx. Postal 467, 19060-900, Presidente Prudente, SP, Brazil

E-mail: marcelo@fct.unesp.br

Received 14 August 2008, in final form 22 January 2009
Published 23 February 2009
Online at stacks.iop.org/JPhysA/42/115101

Abstract

In this paper, by using the Poincaré compactification in $\mathbb{R}^3$ we make a global analysis of the Lorenz system, including the complete description of its dynamic behavior on the sphere at infinity. Combining analytical and numerical techniques we show that for the parameter value $b = 0$ the system presents an infinite set of *singularly degenerate heteroclinic cycles*, which consist of invariant sets formed by a line of equilibria together with heteroclinic orbits connecting two of the equilibria. The dynamical consequences related to the existence of such cycles are discussed. In particular a possibly new mechanism behind the creation of Lorenz-like chaotic attractors, consisting of the change in the stability index of the saddle at the origin as the parameter b crosses the null value, is proposed. Based on the knowledge of this mechanism we have numerically found chaotic attractors for the Lorenz system in the case of small $b > 0$, so nearby the singularly degenerate heteroclinic cycles.

PACS numbers: 05.45.−a, 05.45.Pq, 02.40.Vh
Mathematics Subject Classification: 37C10, 37C29, 37C70

(Some figures in this article are in colour only in the electronic version)

1. Introduction and statement of the results

In this work we make a global analysis of the Lorenz system, given by

$$\dot{x} = \sigma(y - x), \qquad \dot{y} = rx - y - xz, \qquad \dot{z} = -bz + xy, \tag{1}$$

where the state variables $(x, y, z) \in \mathbb{R}^3$ and σ, r and b are real parameters. As usual the dots denote derivative with respect to the time t. System (1) was proposed by the meteorologist Lorenz in 1963 in the study of thermal fluid convection in the atmosphere, related to the question of long-term weather forecasts, see [9]. There are hundreds of papers concerning the

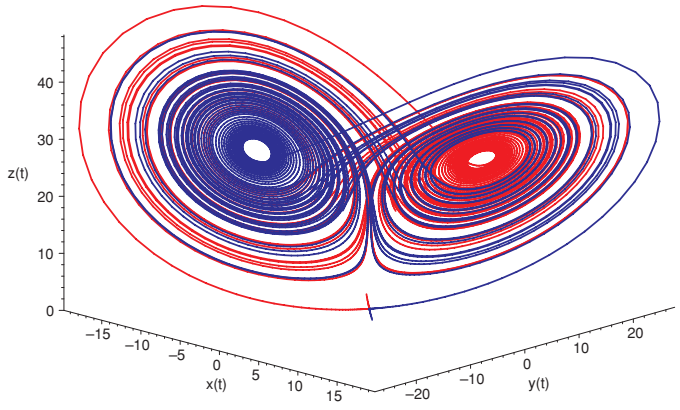

Figure 1. The 'standard' Lorenz attractor.

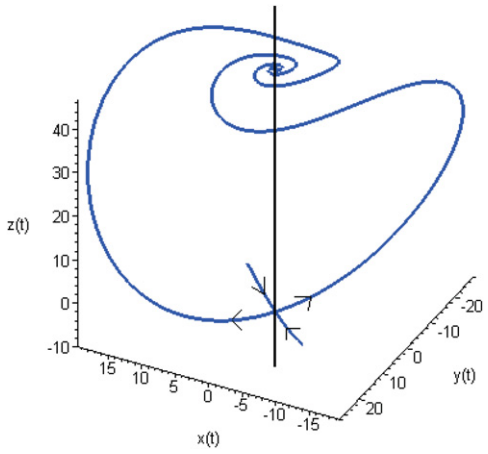

Figure 2. Singularly degenerate heteroclinic cycles of the Lorenz system.

rich dynamical behavior of system (1), see for instance [13] and the more recent work [14] for good reviews on the subject. Most of them consider strictly positive values for the parameters σ, r and b due to their physical meaning. For the classical values $\sigma = 10$, $r = 28$ and $b = 8/3$ the system presents the famous butterfly shaped chaotic attractor shown in figure 1.

For b small and positive (indeed $b = 0.25$) system (1) was studied in chapter 8 of [13], where spiraling behavior of the solutions around the z-axis was described. Also, complex dynamics were observed for large values of the parameter r ($r \geqslant 80$).

In the case of $b = 0, \sigma$ near the classical value 10 and for sufficiently large r (actually, $r \to \infty$) system (1) was analyzed by Kokubu and Roussarie in [7]. In that work the authors proved for a family of three-dimensional ODEs that contains as its subfamily the Lorenz system, the existence of one specific type of heteroclinic cycle, called the *singularly degenerate heteroclinic cycle*. It consists of an invariant set formed by a line of equilibria together with a heteroclinic orbit connecting two of the equilibria (see figure 2). In the case of the Lorenz system studied in [7] the line of equilibria is given by the z-axis, one of the equilibria is the origin and the other one is given by $(0, 0, z^*)$ with z^* sufficiently large (actually, z^* near infinity).

Since the proposal of system (1), several three-dimensional systems of polynomial nonlinear ODEs have been thought about, arising from physical or purely abstract contexts, whose solutions exhibit chaotic dynamics of the Lorenz system type, clearly distinguished by the existence of butterfly shaped attractors. As examples, we can refer to the second Rossler system, Shimizu–Morioka system (see [7] and references therein), Rikitake system [12], Rabinovich system [8, 11] and several others which will pop up in a *MathSciNet* or *Google Scholar* search under the word 'Lorenz'. Because it is one of the first chaotic systems extensively studied, one can say that the Lorenz system has become synonymous with *the chaotic system* as well as the Lorenz attractor of a *strange attractor*, even though several different mathematical definitions for these objects can be found in the literature. These types of chaotic systems are commonly called *Lorenz-like systems*, although the reason for the apparent similarity of their complex dynamics is far from understood.

It was within this context that the authors of [7] suggested, making a comparison with the chaotic Henon map [6], that a basic structure given by some type of 'singular limit' could exist from which the generation of interesting chaotic dynamics could be conceptually understood in all of the Lorenz-like systems. According to the ideas in [7], for the Henon map such a singular structure is rather clear from the expression of the map itself, whereas for the Lorenz system it is not at all obvious what could be such a singular limit, because there can be seen no singular structure from the equations which determine the system. So the authors suggest that, possibly, such a 'singular' and mathematically understandable structure could be provided by the singularly degenerate heteroclinic cycle they have proven to exist for a system equivalent to the Lorenz one, in the case of $b = 0, r \to \infty$ and bounded σ. They also have observed that, due to its degeneracy, the singularly degenerate heteroclinic cycle possibly has a great potential of producing a rich variety of dynamics as shown in the Lorenz system (for more details, see [7], p 527).

In this paper we consider the original Lorenz system (1), instead of an equivalent one, for which we show, combining analytical and numerical studies, that the 'singular structure' behind the solutions of system (1) with $b = 0$ is much more complex than that described in [7]. More precisely, by using the Poincaré compactification for the global analysis of system (1), we give a complete description of its dynamical behavior on the sphere at infinity and make a study of the dynamics in a neighborhood of the infinity. Based on the knowledge of such global structure we carry out a careful numerical analysis of its solutions. The results obtained allow us to conclude that for the parameter values $b = 0$, $\sigma > 1$ and $r > 1$ (not necessarily large) the system presents an infinite set of singularly degenerate heteroclinic cycles, instead of the only one connecting the saddle at the origin with the equilibrium $(0, 0, z^*)$ proved to exist in [7]. Furthermore, we show analytically that a small perturbation in the parameters, simply by considering $b \neq 0$ small, destroys all these singularly degenerate heteroclinic cycles and produces two *infinite heteroclinic orbits*, which consist of two solutions contained in the z-axis connecting the saddle at the origin with equilibrium points at infinity. Also, we numerically found strange attractors for small values of b; hence nearby the singularly degenerate heteroclinic cycles, for several values of the parameters $r > 1$ and bounded $\sigma > 1$ (see figure 3 and also section 5).

The main results in this paper are summarized in the following theorems.

Theorem 1. *For all values of the parameters $r, \sigma, b \in \mathbb{R}$ the phase portrait of system (1) on the sphere at infinity is as shown in figure 4: there exist two centers in the positive and negative endpoints of the x-axis and a circle of equilibria containing the endpoints of the y- and z-axis.*

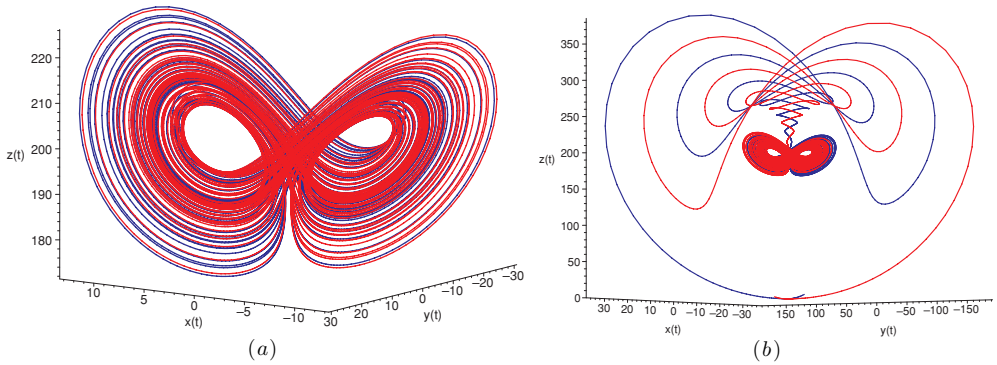

Figure 3. (*a*) Strange attractor of system (1) for the parameter values $b = 0.15, \sigma = 2.3$ and $r = 200$. (*b*) Spiraling behavior of the unstable invariant manifolds of the saddle at the origin around the z-axis, before tending towards the attractor shown in (*a*).

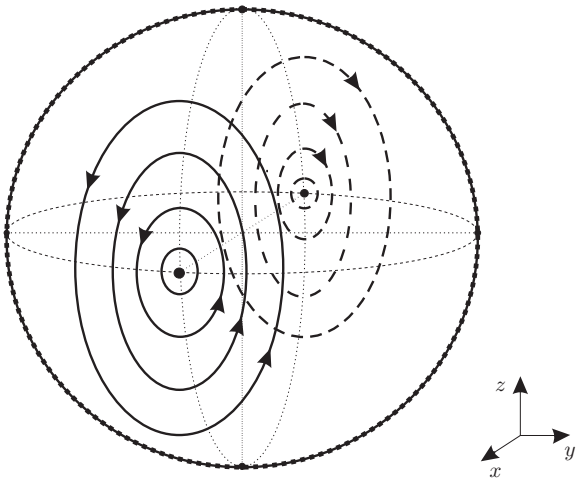

Figure 4. Phase portrait of system (1) at infinity.

It is important to note that the dynamics at infinity do not depend on the parameter values, since the parameters appear only in the linear terms of system (1).

Theorem 2. *The following statements hold for the Lorenz system (1).*

(a) For $b = 0$ and all $r, \sigma \in \mathbb{R}$, system (1) has a line of semi-hyperbolic equilibria, given by the z-axis. Consider $\sigma > 0$ and $r > 1$. Then for $z < r - 1$ the equilibria $P^\star = (0, 0, z)$ are saddles normally hyperbolic to the z-axis, that is the linearized system at $P^\star$ has two real eigenvalues with opposite signs and the corresponding one-dimensional stable and unstable manifolds are normal to the z-axis; for $z > r - 1 + \dfrac{(1+\sigma)^2}{4\sigma}$ the equilibria $Q^\star = (0, 0, z)$ are stable foci normally hyperbolic to the z-axis, that is the linear part of system (1) at $Q^\star$ has complex conjugate eigenvalues with negative real part and corresponding two-dimensional stable manifolds normal to the z-axis.

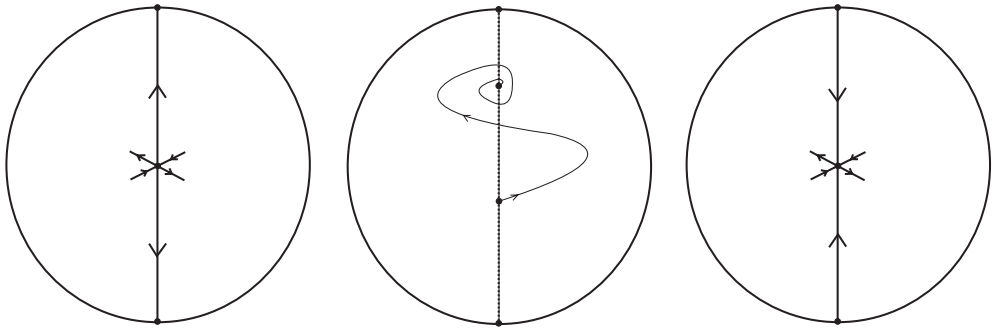

Figure 5. Infinite heteroclinic orbits of system (1) for $b < 0$ (left) and $b > 0$ (right). For $b = 0$ the system has singularly degenerate heteroclinic cycles (center). The boundary of the disks correspond to the points at infinity in the plane yz, see figure 4.

(b) For $b \neq 0$, system (1) has two infinite heteroclinic orbits, one of them consisting of the origin $(0, 0, 0)$, the positive portion of the z-axis and of one equilibrium on the sphere at infinity (the endpoint of the positive z-axis); the other consists of the origin, the negative part of the z-axis and of one equilibrium on the sphere at infinity (the endpoint of the negative z-axis). Moreover, if $b > 0$ the origin is asymptotically stable along the z-axis while for $b < 0$ the origin is unstable (see figure 5).

Based on the results stated in these theorems and through a detailed numerical study we may state the following result.

Numerical Result 3. *For $b = 0, r > 1$ and $\sigma > 1$ the one-dimensional unstable manifolds $W^u(P^\star)$ of each normally hyperbolic saddle $P^\star$ given in part (a) of theorem 2 tend toward one of the normally hyperbolic stable foci $Q^\star$ as $t \to +\infty$, forming singularly degenerate heteroclinic cycles (see figures 2 and 10).*

Numerical result 3 implies that the Lorenz system with $b = 0$ has an infinite set of singularly degenerate heteroclinic cycles instead of the only one proved to exist in [7]. These cycles are studied in section 4.

Furthermore, based on the analytical and numerical results obtained, one can say that, beyond the existence of the singularly degenerate heterolinic cycles themselves, there is a mechanism which plays an important role in the creation of Lorenz-like strange attractors. This mechanism is the change in the stability index of the saddle at the origin when the parameter b crosses the zero value and the degenerate cycles are created. In fact, it is easy to check that, for $b < 0$, the origin is a saddle with a two-dimensional unstable and a one-dimensional stable manifolds (that is, stability index equal to 1); in this case the origin is unstable along the invariant z-axis and consequently the non-vanishing solutions on this axis escape to infinity as $t \to +\infty$ (see figure 5). For $b = 0$, the z-axis becomes a line of equilibria and the singularly degenerate heterolinic cycles are created. For $b > 0$, the origin is a saddle with a two-dimensional stable and a one-dimensional unstable manifolds (that is, stability index equal to 2); in this case the origin becomes stable along the invariant z-axis (see figure 5 again). Furthermore, for $b > 0$ small two new stable equilibria arise as well as the origin, which are given by (see [13])

$$Q_\pm = (\pm\sqrt{b(r-1)}, \pm\sqrt{b(r-1)}, r-1)).$$

This change in the stability index of the origin, in addition to the creation of the two new equilibria, makes the unbounded solutions which tend to infinity come back to a neighborhood of the origin, tending initially to these stable equilibria and then to the bounded strange attractor, as b is varied. Indeed, if $b < 0$ it is impossible for an ellipsoid bounding the solutions of system (1) to exist, since the non-vanishing solutions on the z-axis escape to infinity. On the other hand, such an ellipsoid does exist for $b > 0$, under certain conditions on the parameters values, as described for example, in [4] and [13]. This ellipsoid contains a strange attractor, when it exists.

The existence of an infinite set of singularly degenerate heteroclinic cycles and the occurrence of strange attractors nearby have recently been described in [8] and [10] in the study of other quadratic nonlinear systems of ODEs in $\mathbb{R}^3$.

Finally we observe that the aim of the present work is, through a global analysis by using the Poincaré compactification combined with a numerical study, to bring a contribution in the understanding of the Lorenz system with small b, which is in general a hard task. Indeed, as said in Sparrow's book [13], p 177: 'the Lorenz system for small b is one of the most complicated three-dimensional chaotic systems of ordinary differential equations ever observed (if not the most), and attempts at complete understanding are almost certainly doomed'. Moreover, although being applied only to the analysis of the Lorenz system, the techniques used in this note may be applied in the analysis of other polynomial differential systems and we believe that they provide useful tools for the understanding of dynamical phenomena in the state space $\mathbb{R}^3$.

The paper is organized as follows: in section 2 for the sake of completeness we present the Poincaré compactification for a polynomial vector field in $\mathbb{R}^3$, which allows us to study in section 3 the dynamics of the Lorenz system in a neighborhood of and on the sphere at infinity and consequently to prove theorem 1. Based on the knowledge of the dynamical behavior near and at infinity, in section 4 we prove theorem 2 and present the numerical study which leads to numerical result 3. Finally, in section 5 numerically computed strange attractors for small values of the parameter b are presented.

2. Poincaré compactification in $\mathbb{R}^3$

A polynomial vector field X in $\mathbb{R}^n$ can be extended to a unique analytic vector field on the sphere $\mathbb{S}^n$. The technique for making such an extension is called the Poincaré compactification and allows us to study a polynomial vector field in a neighborhood of infinity, which corresponds to the equator $\mathbb{S}^{n-1}$ of the sphere $\mathbb{S}^n$. Poincaré introduced this compactification for polynomial vector fields in $\mathbb{R}^2$. Its extension to $\mathbb{R}^n$ for $n > 2$ can be found in [3]. In this section, we describe the Poincaré compactification for polynomial vector fields in $\mathbb{R}^3$ following closely what is made in [3].

In $\mathbb{R}^3$ we consider the polynomial differential system

$$\dot{x} = P^1(x, y, z), \qquad \dot{y} = P^2(x, y, z), \qquad \dot{z} = P^3(x, y, z),$$

or equivalently its associated polynomial vector field $X = (P^1, P^2, P^3)$. The degree n of X is defined as $n = \max\{\deg(P^i) : i = 1, 2, 3\}$.

Let $\mathbb{S}^3 = \{y = (y_1, y_2, y_3, y_4) \in \mathbb{R}^4 : \|y\| = 1\}$ be the unit sphere in $\mathbb{R}^4$, and $\mathbb{S}_+ = \{y \in \mathbb{S}^3 : y_4 > 0\}$ and $\mathbb{S}_- = \{y \in \mathbb{S}^3 : y_4 < 0\}$ be the northern and southern hemispheres of $\mathbb{S}^3$, respectively. The tangent space to $\mathbb{S}^3$ at the point y is denoted by $T_y\mathbb{S}^3$. Then the tangent plane

$$T_{(0,0,0,1)}\mathbb{S}^3 = \{(x_1, x_2, x_3, 1) \in \mathbb{R}^4 : (x_1, x_2, x_3) \in \mathbb{R}^3\}$$

is identified with $\mathbb{R}^3$.

We consider the central projections $f_+ : \mathbb{R}^3 = T_{(0,0,0,1)}\mathbb{S}^3 \longrightarrow \mathbb{S}_+$ and $f_- : \mathbb{R}^3 = T_{(0,0,0,1)}\mathbb{S}^3 \longrightarrow \mathbb{S}_-$ defined by $f_\pm(x) = \pm(x_1, x_2, x_3, 1)/\Delta x$, where $\Delta x = \left(1 + \sum_{i=1}^3 x_i^2\right)^{1/2}$. Through these central projections $\mathbb{R}^3$ is identified with the northern and southern hemispheres of $\mathbb{S}^3$. The equator of $\mathbb{S}^3$ is $\mathbb{S}^2 = \{y \in \mathbb{S}^3 : y_4 = 0\}$. Clearly $\mathbb{S}^2$ can be identified with the infinity of $\mathbb{R}^3$.

The maps f_+ and f_- define two copies of X on $\mathbb{S}^3$, one $Df_+ \circ X$ in the northern hemisphere and the other $Df_- \circ X$ in the southern one. Denoted by $\overline{X}$ the vector field on $\mathbb{S}^3 \setminus \mathbb{S}^2 = \mathbb{S}_+ \cup \mathbb{S}_-$ which, restricted to $\mathbb{S}_+$ coincides with $Df_+ \circ X$ and restricted to $\mathbb{S}_-$ coincides with $Df_- \circ X$.

The expression for $\overline{X}(y)$ on $\mathbb{S}_+ \cup \mathbb{S}_-$ is

$$\overline{X}(y) = y_4 \begin{pmatrix} 1 - y_1^2 & -y_2 y_1 & -y_3 y_1 \\ -y_1 y_2 & 1 - y_2^2 & -y_3 y_2 \\ -y_1 y_3 & -y_2 y_3 & 1 - y_3^2 \\ -y_1 y_4 & -y_2 y_4 & -y_3 y_4 \end{pmatrix} \begin{pmatrix} P^1 \\ P^2 \\ P^3 \end{pmatrix},$$

where $P^i = P^i\,(y_1/|y_4|, y_2/|y_4|, y_3/|y_4|)$. Written in this way $\overline{X}(y)$ is a vector field in $\mathbb{R}^4$ tangent to the sphere $\mathbb{S}^3$.

Now we can extend analytically the vector field $\overline{X}(y)$ to the whole sphere $\mathbb{S}^3$ by $p(X)(y) = y_4^{n-1}\overline{X}(y)$. This extended vector field $p(X)$ is called the Poincaré compactification of X on $\mathbb{S}^3$.

As $\mathbb{S}^3$ is a differentiable manifold in order to compute the expression for $p(X)$ we can consider the eight local charts (U_i, F_i), (V_i, G_i), where $U_i = \{y \in \mathbb{S}^3 : y_i > 0\}$ and $V_i = \{y \in \mathbb{S}^3 : y_i < 0\}$ for $i = 1, 2, 3, 4$; the diffeomorphisms $F_i : U_i \to \mathbb{R}^3$ and $G_i : V_i \to \mathbb{R}^3$ for $i = 1, 2, 3, 4$ are the inverses of the central projections from the origin to the tangent planes at the points $(\pm1, 0, 0, 0)$, $(0, \pm1, 0, 0)$, $(0, 0, \pm1, 0)$ and $(0, 0, 0, \pm1)$, respectively. Now we do the computations on U_1. Suppose that the origin $(0, 0, 0, 0)$, the point $(y_1, y_2, y_3, y_4) \in \mathbb{S}^3$ and the point $(1, z_1, z_2, z_3)$ in the tangent plane to $\mathbb{S}^3$ at $(1, 0, 0, 0)$ are collinear. Then we have $1/y_1 = z_1/y_2 = z_2/y_3 = z_3/y_4$, and consequently $F_1(y) = (y_2/y_1, y_3/y_1, y_4/y_1) = (z_1, z_2, z_3)$ defines the coordinates on U_1. As

$$DF_1(y) = \begin{pmatrix} -y_2/y_1^2 & 1/y_1 & 0 & 0 \\ -y_3/y_1^2 & 0 & 1/y_1 & 0 \\ -y_4/y_1^2 & 0 & 0 & 1/y_1 \end{pmatrix}$$

and $y_4^{n-1} = (z_3/\Delta z)^{n-1}$, the analytical vector field $p(X)$ becomes

$$\frac{z_3^n}{(\Delta z)^{n-1}}(-z_1 P^1 + P^2, -z_2 P^1 + P^3, -z_3 P^1),$$

where $P^i = P^i\,(1/z_3, z_1/z_3, z_2/z_3)$.

In a similar way we can deduce the expressions of $p(X)$ in U_2 and U_3. These are

$$\frac{z_3^n}{(\Delta z)^{n-1}}(-z_1 P^2 + P^1, -z_2 P^2 + P^3, -z_3 P^2),$$

where $P^i = P^i(z_1/z_3, 1/z_3, z_2/z_3)$ in U_2, and

$$\frac{z_3^n}{(\Delta z)^{n-1}}(-z_1 P^3 + P^1, -z_2 P^3 + P^2, -z_3 P^3),$$

where $P^i = P^i(z_1/z_3, z_2/z_3, 1/z_3)$ in U_3.

The expression for $p(X)$ in U_4 is $z_3^{n+1}(P^1, P^2, P^3)$, now denoting $P^i = P^i(z_1, z_2, z_3)$. The expression for $p(X)$ in the local chart V_i is the same as in U_i multiplied by $(-1)^{n-1}$.

When we work with the expression of the compactified vector field $p(X)$ in the local charts we usually omit the factor $1/(\Delta z)^{n-1}$. We can do that through a rescaling of the time variable.

In what follows, we shall work with the orthogonal projection of $p(X)$ from the closed northern hemisphere to $y_4 = 0$, we continue denoting this projected vector field by $p(X)$. Note that the projection of the closed northern hemisphere is a closed ball B of radius one, whose interior is diffeomorphic to $\mathbb{R}^3$ and whose boundary $\mathbb{S}^2$ corresponds to the infinity of $\mathbb{R}^3$. Of course $p(X)$ is defined in the whole closed ball B in such a way that the flow on the boundary is invariant. This new vector field on B will be called the *Poincaré compactification* of X, and B will be called the *Poincaré ball*.

Remark 4. All the points on the invariant sphere $\mathbb{S}^2$ at infinity in the coordinates of any local chart U_i and V_i have $z_3 = 0$. Also, the points in the interior of the Poincaré ball, which is diffeomorphic to $\mathbb{R}^3$, are given in the local charts U_1, U_2 and U_3 by $z_3 > 0$ and in the local charts V_1, V_2 and V_3 by $z_3 < 0$. These half-spaces will be considered in the study of the flow of system (1) in a neighborhood of the infinite sphere later on.

3. Behavior of system (1) near and at infinity

In this section we shall make an analysis of the flow of system (1) near and at infinity. In order to do so in the following four subsections we shall analyze the Poincaré compactification of the system in the local charts U_i and V_i, $i = 1, 2, 3$.

3.1. In the local charts U_1 *and* V_1

From the results of section 2 the expression of the Poincaré compactification $p(X)$ of system (1) in the local chart U_1 is given by

$$\begin{aligned} \dot{z_1} &= -z_2 + rz_3 - z_1z_3 - \sigma z_1^2 z_3 + \sigma z_1 z_3, \\ \dot{z_2} &= z_1 - bz_2z_3 + \sigma z_2 z_3 - \sigma z_1 z_2 z_3, \\ \dot{z_3} &= -\sigma z_3^2(z_1 - 1). \end{aligned} \tag{2}$$

For $z_3 = 0$ (which corresponds to the points on the sphere $\mathbb{S}^2$ at infinity) the unique equilibrium point of (2) is $(0, 0, 0)$ and the eigenvalues of the linear part of the system at this point are i, $-i$ and 0.

In general, the dynamics near a non-hyperbolic equilibrium point of this type can be rather complex, see for instance [5]. Fortunately as a property of the compactification procedure, the plane z_1z_2 is invariant under the flow of system (2), which makes the analysis on the sphere at infinity simpler. Taking $z_3 = 0$ equations (2) reduce to

$$\dot{z_1} = -z_2, \qquad \dot{z_2} = z_1, \tag{3}$$

which has a linear center at the origin. Consequently system (1) has, after compactification, a center on the sphere at infinity at the positive endpoint of the x-axis (see figure 4).

The flow in the local chart V_1 is the same as the flow in the local chart U_1 reversing the time, because the compactified vector field $p(X)$ in V_1 coincides with the vector field $p(X)$ in U_1 multiplied by -1 (for details see section 2). Hence system (1) also has a center on the infinite sphere at the negative endpoint of the x-axis (see figure 4 again).

Now we will study the dynamics of system (1) in a neighborhood of the infinite sphere on the local charts U_1 and V_1, aiming to understand how the solutions come from and go to infinity. In order to do so we will consider firstly $z_3 > 0$ small (see remark 4). The unique equilibrium point of (2) is $p_1 = (0, 0, 0)$ and the eigenvalues of the linearized system at this point are $i, -i$ and 0, the zero eigenvalue having eigenvector $(0, r, 1)$. The pure imaginary eigenvalues correspond to the center at infinity. Hence from the center manifold theorem (see [1] or [2]) the system has a one-dimensional center manifold to p_1 contained in the interior of the ball diffeomorphic to $\mathbb{R}^3$, corresponding to $z_3 > 0$. The following proposition holds.

Proposition 5. *The singular point $p_1 = (0, 0, 0)$ of system (2) is locally asymptotically unstable along its one-dimensional center manifold.*

Proof. Under the above considerations, from the center manifold theorem (see [1] or [2]) it follows that system (2) has a one-dimensional center manifold to the singular point $p_1 = (0, 0, 0)$, which is the graph of a function $h : \mathbb{R} \to \mathbb{R}^2$ given by $(z_1, z_2) = h(z_3) = (h_1(z_3), h_2(z_3))$ satisfying the conditions

$$h(0) = (0, 0), \qquad Dh(0) = (0, r), \tag{4}$$

and

$$\dot{z}_1 - Dh_1(z_3)\dot{z}_3 = 0, \qquad \dot{z}_2 - Dh_2(z_3)\dot{z}_3 = 0. \tag{5}$$

Moreover the flow on this center manifold is governed by the one-dimensional equation

$$\dot{z}_3 = -\sigma z_3^2(h_1(z_3) - 1). \tag{6}$$

To understand the flow on this manifold we will obtain an approximation of the function h by expanding it in Taylor series around $z_3 = 0$ to the fourth order using conditions (4), that is

$$h_1(z_3) = \sum_{i=2}^{4} a_i z_3^i \qquad \text{and} \qquad h_2(z_3) = r z_3 + \sum_{i=2}^{4} b_i z_3^i. \tag{7}$$

Now from (5) and considering the expressions for $\dot{z}_1$ and $\dot{z}_2$ given by system (2) we have

$$\begin{aligned} &-h_2 + r z_3 - h_1 z_3 - \sigma h_1^2 z_3 + \sigma h_1 z_3 - Dh_1\big(-\sigma z_3^2(h_1 - 1)\big) = 0,\\ &h_1 - b h_2 z_3 + \sigma h_2 z_3 - \sigma h_1 h_2 z_3 - Dh_2\big(-\sigma z_3^2(h_1 - 1)\big) = 0, \end{aligned} \tag{8}$$

where $h_1 = h_1(z_3)$ and $h_2 = h_2(z_3)$ are provided by (7) and $Dh_i = h_i'(z_3)$, $i = 1, 2$. Equating the powers of z_3 coefficients in (8) we obtain

$$\begin{aligned} &a_2 = br, \qquad a_3 = 0 \qquad \text{and} \qquad a_4 = -br(b + 2\sigma)(\sigma + 1)\\ &b_2 = 0, \qquad b_3 = -br(\sigma + 1) \qquad \text{and} \qquad b_4 = 0. \end{aligned}$$

Then we have the following approximation for the central manifold h:

$$h(z_3) = (h_1(z_3), h_2(z_3)),$$

where

$$h_1(z_3) = br z_3^2 - br(\sigma + 1)(b + 2\sigma) z_3^4 + O\big(z_3^6\big)$$

and

$$h_2(z_3) = r z_3 - br(\sigma + 1) z_3^3 + O\big(z_3^5\big).$$

Substituting the expression of $h_1(z_3)$ into equation (6) it follows that the flow on the center manifold is governed by the equation

$$\dot{z}_3 = -\sigma z_3^2\left[br z_3^2 - br(\sigma + 1)(b + 2\sigma) z_3^4 + O\big(z_3^6\big) - 1\right] = \sigma z_3^2 + O\big(z_3^4\big).$$

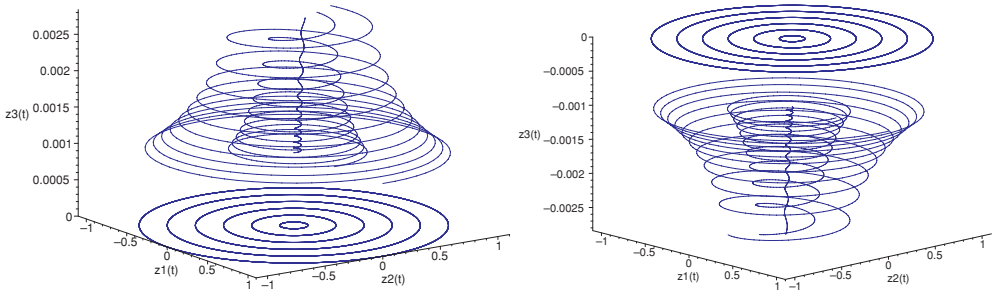

(*a*) (*b*)

Figure 6. Dynamics of system (1) near the sphere at infinity in the local charts U_1 (*a*) and V_1 (*b*): there are one-dimensional unstable center manifolds to the origin in both charts; the solutions starting near the periodic orbits of the centers at infinity go far from them.

Since $\sigma > 0$ and we are considering $z_3 > 0$ small, it implies that p_1 is locally asymptotically unstable along its center manifold. □

As the flow in the local chart V_1 is the same as the flow in the local chart U_1 reversing the time (see section 2), under the same arguments stated above, we can deduce that the flow on the center manifold of the origin in the local chart V_1 is governed by the equation

$$\dot{z}_3 = -\sigma z_3^2 + O\left(z_3^4\right).$$

Hence, as in the vicinity of the infinity in the local chart V_3 we have $z_3 < 0$ (see remark 4), it implies that the origin on the local chart V_1 is also locally asymptotically unstable along its center manifold.

In short, the equilibria at infinity at the positive and negative endpoints of the x-axis are unstable along their one-dimensional center manifolds. However this analysis is not enough to describe completely the behavior of the solutions in a neighborhood of the infinite sphere in the local charts U_1 and V_1. In fact, it could happen that a solution enter the infinity tending to one of the periodic orbits of the centers at infinity. Then, in order to complete the analysis, we have used numerical simulations for several values of the parameters and different initial conditions, which indicate that the periodic orbits at infinity are normally unstable, that is any solution starting in the interior of the Poincaré ball and near any periodic orbit of the centers at infinity go far from them (see figure 6), following the behavior on the center manifolds described above.

3.2. In the local charts U_2 *and* V_2

Again using the results stated in section 2 we have that the expression of the Poincaré compactification $p(X)$ of system (1) in the local chart U_2 is given by

$$\begin{aligned}
\dot{z}_1 &= \sigma z_3 + z_1 z_3 - \sigma z_1 z_3 + z_1^2 z_2 - r z_1^2 z_3,\\
\dot{z}_2 &= z_1 - b z_2 z_3 + z_1 z_2^2 + z_2 z_3 - r z_1 z_2 z_3,\\
\dot{z}_3 &= -z_3(r z_1 z_3 - z_3 - z_1 z_2).
\end{aligned} \tag{9}$$

If $z_3 = 0$ system (9) has a line of equilibria given by the z_2-axis and the linear part of the system at these equilibria has three null eigenvalues. Using the invariance of the plane $z_1 z_2$ under the flow of (9) we can completely describe the dynamics on the sphere at infinity. In fact, if $z_3 = 0$ the system reduces to

$$\dot{z}_1 = z_1^2 z_2, \qquad \dot{z}_2 = z_1 + z_1 z_2^2, \tag{10}$$

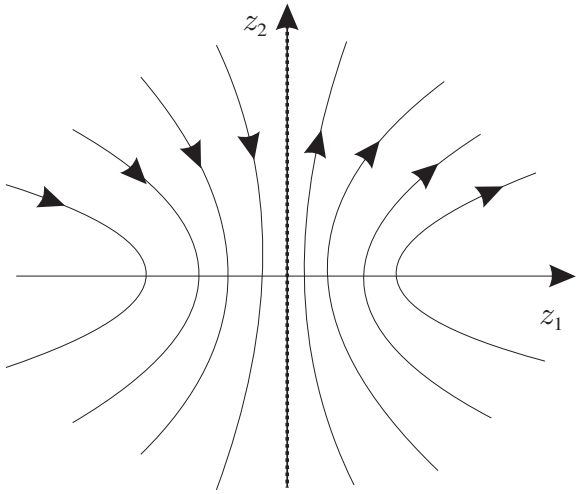

Figure 7. Phase portrait of system (10), which corresponds to the phase portrait of system (1) at infinity in the local chart U_1.

which is an integrable system, since if $z_1 \neq 0$ it has the first integral

$$H(z_1, z_2) = \ln|z_1| - \tfrac{1}{2}\ln\left(1 + z_2^2\right).$$

Using this first integral and observing that system (10) has the z_2-axis as a line of equilibria, we have that the global phase portrait in the local chart U_2 on the infinite sphere is as shown in figure 7.

The flow in the local chart V_2 is the same as the flow in the local chart U_2 reversing the time, because the compactified vector field $p(X)$ in V_2 coincides with the vector field $p(X)$ in U_2 multiplied by -1. Hence the phase portrait on the chart V_2 is the same as shown in figure 7, reversing appropriately the time direction.

For $z_3 > 0$ small, which correspond to the points in the interior of the Poincaré ball, the solutions behave like those shown in figure 8.

3.3. In the local charts U_3 *and* V_3

The expression of the Poincaré compactification $p(X)$ in the local chart U_3 is

$$\begin{aligned}
\dot{z}_1 &= \sigma z_2 z_3 - \sigma z_1 z_3 - z_1^2 z_2 + b z_1 z_3,\\
\dot{z}_2 &= -z_1 - z_2 z_3 + r z_1 z_3 - z_1 z_2^2 + b z_2 z_3,\\
\dot{z}_3 &= z_3(b z_3 - z_1 z_2).
\end{aligned} \tag{11}$$

For $z_3 = 0$, system (11) reduces to equations (10) multiplied by -1 and hence the analysis on the sphere at infinity is the same as the one made in the previous subsection.

Now we shall study system (11) in a neighborhood of the infinite sphere on the chart U_3, by considering $z_3 > 0$ small, since we are interested in the behavior of the solutions which tend to infinity on the z-axis. Indeed it will be used in the proof of theorem 2 in the following section.

The z_3-axis is invariant by the flow of (11), since for $z_1 = z_2 = 0$ the system reduces to

$$\dot{z}_1 = 0, \qquad \dot{z}_2 = 0, \qquad \dot{z}_3 = b z_3^2,$$

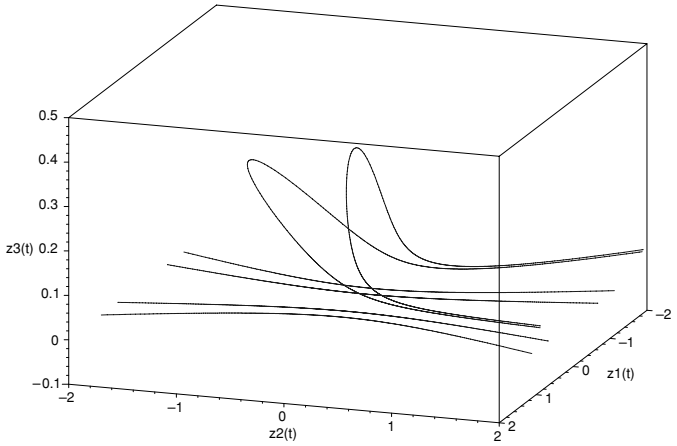

Figure 8. Dynamics of system (1) near the sphere at infinity in the local charts U_2 and V_2: there is no periodic orbits; the solutions turn its direction when crossing the plane $z_1 = 0$.

hence the origin is asymptotically stable (resp. unstable) if $b < 0$ (resp. $b > 0$). Furthermore, if $b = 0$ then the system has a line of equilibria in the z_3-axis and the following proposition holds.

Proposition 6. *The equilibrium points* $(0, 0, z_3)$ *of system (11) are stable spirals normally hyperbolic to the* z_3*-axis, that is the linear part of the system at each equilibria* $(0, 0, z_3)$ *has complex conjugate eigenvalues with negative real part and the corresponding two-dimensional stable manifolds normal to the* z_3*-axis, provided the following condition holds*

$$\frac{1}{z_3} > r + \frac{(\sigma - 1)^2}{4\sigma}. \tag{12}$$

Proof. For $b = 0$ the Jacobian matrix of system (11) at the unique equilibrium point $(0, 0, z_3)$ is given by

$$\begin{pmatrix} -\sigma z_3 & \sigma z_3 & 0 \\ r z_3 - 1 & -z_3 & 0 \\ 0 & 0 & 0 \end{pmatrix},$$

which has the eigenvalues

$$\lambda_{1,2} = -\frac{z_3(\sigma + 1)}{2} \pm \frac{\sqrt{z_3^2(\sigma + 1)^2 - 4\sigma\left(z_3^2 - r z_3^2 + z_3\right)}}{2}, \qquad \lambda_3 = 0$$

with corresponding eigenvectors

$$v_{1,2} = \left(z_3(1 - \sigma) \pm \sqrt{z_3^2(\sigma - 1)^2 + 4\sigma\left(z_3^2 r - z_3\right)}, 2, 0\right) \qquad v_3 = (0, 0, 1),$$

from which the proposition follows, since we consider $\sigma > 0$ and $z_3 > 0$. □

The flow in the local chart V_3 is the same as the flow in the local chart U_3 reversing the time. So the same type of analysis as made above, taking into account that near the infinity in the local chart V_3 we have $z_3 < 0$ (see remark 4), allows us to prove the following preposition. We can prove the following proposition.

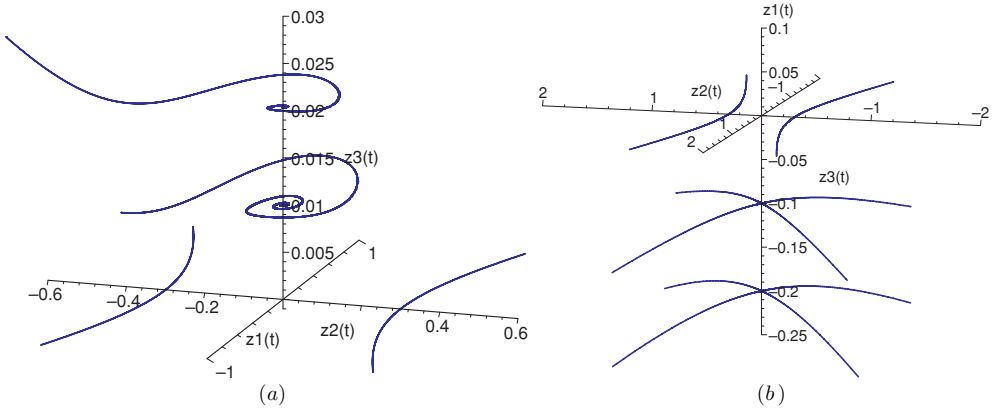

Figure 9. Behavior of the solutions of system (1) with $b = 0$ near the sphere at infinity: $(0, 0, z_3)$ are stable spirals normal to the z_3-axis in the local chart U_3 (left) and normally hyperbolic saddles in the local chart V_3 (right).

Proposition 7. *The equilibrium points* $(0, 0, z_3)$ *of system (11) with reversed time (that is in the local chart* V_3*) are saddles normally hyperbolic to* z_3*-axis, that is the linear part of the system at each equilibrium* $(0, 0, z_3)$ *has two real eigenvalues with opposite signs and the corresponding one-dimensional stable and unstable manifolds normal to the* z_3*-axis.*

From the propositions above we have that near infinity in the chart U_3, that is for $z_3 > 0$ small, the solutions behave like those shown in figure 9(*a*). Near infinity in the chart V_3, that is for $z_3 < 0$ small, the solutions behave like those shown in figure 9(*b*).

3.4. Dynamic of system (1) on the sphere at infinity

Putting together the analysis made in the previous subsections we have a global picture of the dynamical behavior of system (1) on the sphere at infinity: the system has two linear centers, localized at the endpoints of the x-axis, and one circle of equilibria containing the endpoints of the y- and z- axis (see figure 4). This proves theorem 1. It is important to note that the dynamics at infinity does not depend on the values of the parameters σ, r or b.

We observe that the description of the complete phase portrait of system (1) on the sphere at infinity was possible because of the invariance of this set under the flow of the compactified system.

4. Heteroclinic cycles

4.1. Singularly degenerate heteroclinic cycles

For $b = 0$, the Lorenz system (1) reduces to

$$\dot{x} = \sigma(y - x), \qquad \dot{y} = rx - y - xz, \qquad \dot{z} = xy, \tag{13}$$

which has the line of equilibria $(0, 0, z)$, $z \in \mathbb{R}$. Remember we are considering $\sigma > 1$ and $r > 1$. The Jacobian matrix of system (13) at the equilibrium point $(0, 0, z)$ is given by

$$\begin{pmatrix} -\sigma & \sigma & 0 \\ r - z & -1 & 0 \\ 0 & 0 & 0 \end{pmatrix},$$

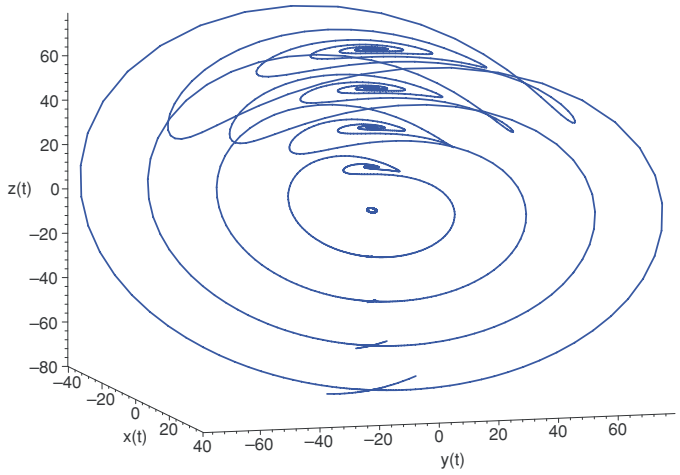

Figure 10. Singularly degenerate heteroclinic cycles of the Lorenz system (1) with $b = 0$, $\sigma = 10, r = 2$. Time of integration: $[-0.4, 10]$. Initial conditions: $(0.01, 0.01, z(0))$ and $(-0.01, -0.01, z(0))$, where $z(0) \in \{0, -20, -40, -60, -80\}$. Stepsize $= 0.005$.

which has the eigenvalues

$$\lambda_{1,2} = -\frac{\sigma+1}{2} \pm \frac{\sqrt{(\sigma+1)^2 + 4\sigma(r-z-1)}}{2}, \qquad \lambda_3 = 0$$

with corresponding eigenvectors

$$v_{1,2} = \left((1-\sigma) \pm \sqrt{(\sigma-1)^2 + 4\sigma(r-z)}, 2(r-z), 0\right) \qquad v_3 = (0,0,1).$$

Providing $z > r - 1 + \dfrac{(\sigma+1)^2}{4\sigma}$, the eigenvalues $\lambda_{1,2}$ are complex with the negative real part. Considering also the corresponding eigenvectors, this implies that the solutions locally spiraling toward the equilibrium point $Q^\star = (0, 0, z)$ on a surface tangent to the plane spanned by the eigenvectors $v_{1,2}$, hence in a direction normal to the z-axis. If $r - 1 + \dfrac{(\sigma+1)^2}{4\sigma} > z > r - 1$, then the eigenvalues $\lambda_{1,2}$ are real and negative. Hence, trajectories move toward the z-axis without spiraling. For $z < r - 1$, the eigenvalues $\lambda_{1,2}$ are real with opposite signs. Then taking into account the eigenvectors $v_{1,2}$, the system has a normally hyperbolic saddle at the point $P^\star = (0, 0, z)$. In the specific case in which $z = r - 1$ the equilibrium point $(0, 0, z)$ is more degenerated, having two vanishing eigenvalues. From these considerations the proof of statement (a) of theorem 2 follows.

A detailed numerical study of the solutions of system (1) with $b = 0, \sigma > 1$ and $r > 1$ has been made, which clearly indicate that the system present an infinite set of singularly degenerate heteroclinic cycles. Each one of these cycles is formed by one of the one-dimensional unstable manifolds of the saddle $P^\star$, which connects $P^\star$ with the normally hyperbolic focus $Q^\star$, as $t \to +\infty$. As the system presents an infinite number of normally hyperbolic saddles $P^\star$ and foci $Q^\star$, there exists an infinite set of singularly degenerate heteroclinic cycles. In figures 10, 11 and 12 some of them are shown: for each initial condition considered sufficiently close to the saddle $P^\star$ at the z-axis, a singularly degenerate heteroclinic cycle is created.

We observe that the saddles $P^\star$ and the stable foci $Q^\star$ extend to infinity on the negative and positive parts of the z-axis, respectively, as shown in the analysis made near and at infinity in section 3.

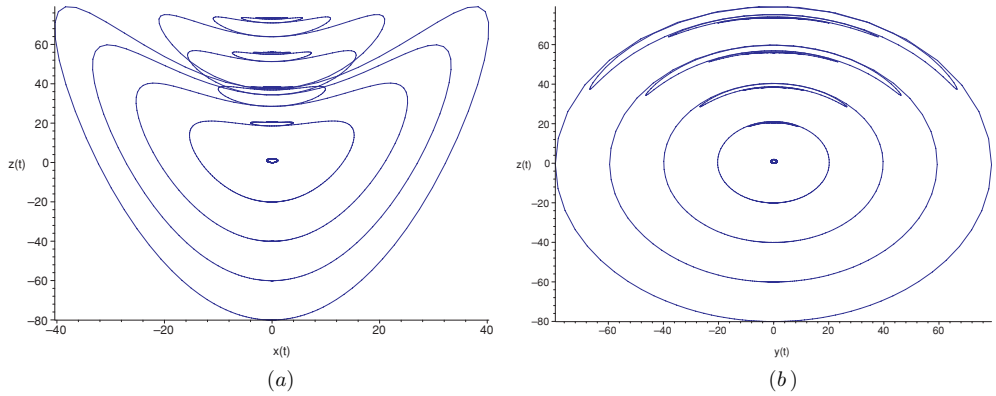

Figure 11. Projections of figure 10 on the planes xz (a) and yz (b).

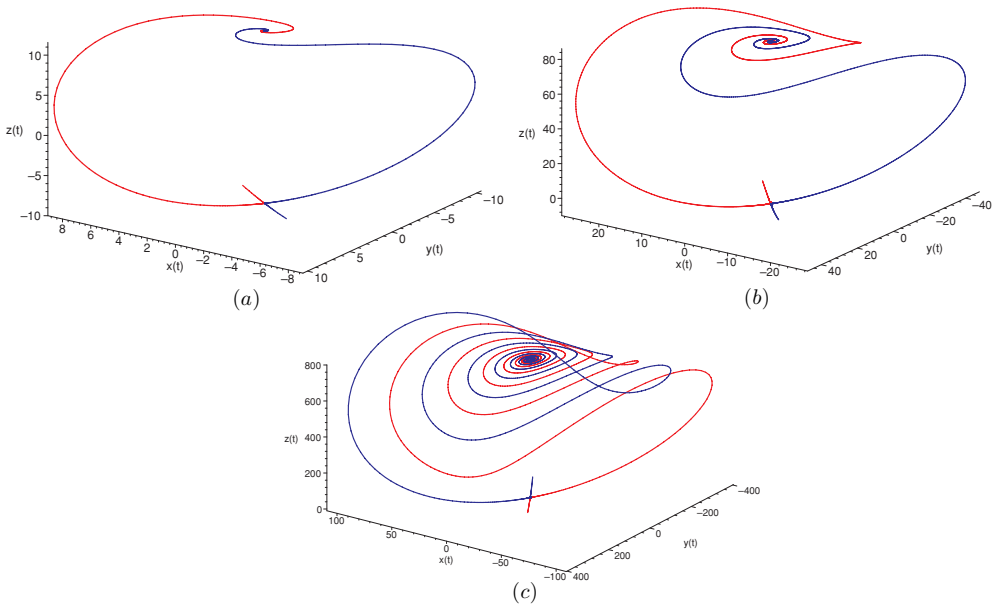

Figure 12. Singularly degenerate heteroclinic cycles of system (1) with $b = 0, \sigma = 10$ and: (a) $r = 2$, (b) $r = 40$ and (c) $r = 400$.

There is nothing special about the values of the parameters σ and r considered to generate the singularly degenerate heteroclinic cycles shown in figure 10. Another values produce the same type of cycles, provided we take $b = 0$. We emphasize only that the increasing values of the parameter r causes an increase in the number of turns that $W^u(P^\star)$ makes around the z-axis, before tending toward $Q^\star$, as shown in figure 12.

The numerical results are also in agreement with the statements in [7]. Namely, they have proven that for $b = 0$ and sufficiently large r there exists a singularly degenerate heteroclinic cycle connecting the saddle at the origin with the normally hyperbolic focus $(0, 0, z^*)$, for large z^*. We verified this fact numerically. For example, take $r = 20000$ and the initial conditions on the unstable manifolds of the saddle at the origin. In this case we have $Q^\star = (0, 0, z^\star)$

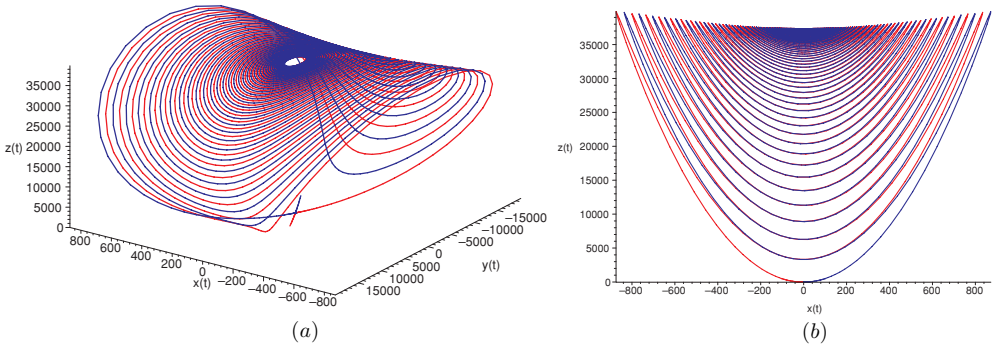

Figure 13. (*a*) Singularly degenerate heteroclinic cycle of system (1) with $b = 0, \sigma = 10$ and $r = 20000$ and (*b*) its projection on the plane xz.

with $z^\star$ approximately equal to 40 000 (see figure 13). Observe also the increasing number of turns in the spiraling behavior of the solutions around the z-axis.

From the considerations above the numerical result 3 is verified.

4.2. Infinite heteroclinic orbits

For $b \neq 0$ small, $r > 1$ and $\sigma > 1$, system (1) has a saddle point at the origin, which is the unique equilibrium point on the z-axis. The Jacobian matrix at this point has the eigenvalues

$$\lambda_{1,2} = -\frac{\sigma+1}{2} \pm \frac{\sqrt{(\sigma+1)^2 - 4\sigma(1-r)}}{2}, \qquad \lambda_3 = -b$$

with corresponding eigenvectors

$$v_{1,2} = \left((1-\sigma) \pm \sqrt{(1-\sigma)^2 + 4\sigma r}, 2r, 0\right), \qquad v_3 = (0, 0, 1).$$

Hence, for $b < 0$, the stability index of the saddle is 1. It is easy to check that the z-axis is invariant under the flow of system (1) and from the calculations above it follows that the origin is unstable along this axis. Moreover, the equilibria at the endpoints of the z-axis on the sphere at infinity, which coincide with the origin in the local charts U_3 and V_3, are asymptotically stable (see, subsection 3.3). Thus system (1) has two infinite heteroclinic orbits, one of them consisting of the origin, the positive portion of the z-axis and of one equilibrium on the sphere at infinity (the endpoint of the positive z-axis); the other one consists of the origin, the negative part of the z-axis and of the endpoint of the negative z-axis (see figure 5).

For $b > 0$, the stability index of the saddle is 2, the origin is asymptotically stable along the z-axis while the endpoints of this axis on the sphere at infinity are unstable (see, subsection 3.3). Again the system has two infinite heteroclinic orbits on the z-axis (see figure 5).

From these considerations we have proven statement (b) of theorem 2.

5. The existence of Lorenz-like attractors for *b* near zero

Through the numerical study carried out, we found Lorenz-like strange attractors of system (1) for several values of the parameters $r > 1$ and $\sigma > 1$, near the singularly degenerate heteroclinic cycles which exist for $b = 0$. In figure 14(*a*) it is shown one of them, obtained for $b = 0.15, \sigma = 2.3$ and $r = 7.8$. We have taken the same parameter values and compute

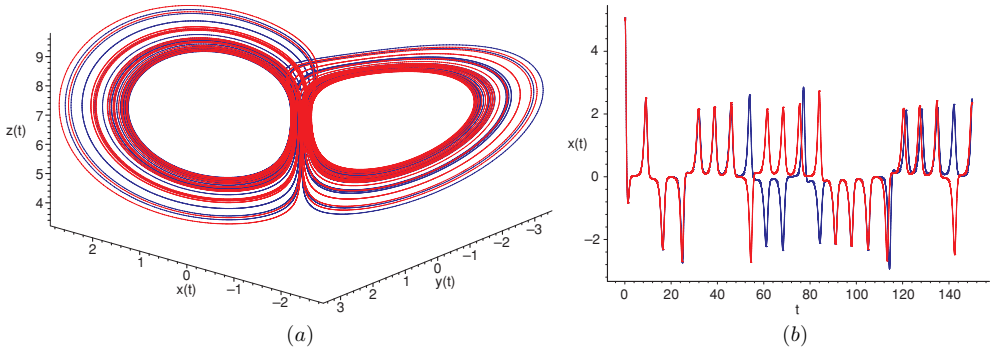

(*a*) (*b*)

Figure 14. (*a*) Strange attractor created through the elimination of the singularly degenerate heteroclinic cycles. Parameter values $b = 0.15, \sigma = 2.3$ and $r = 7.8$; (*b*) its x-coordinate $(t, x(t))$ with initial conditions $(5, 5, 5)$ and $(5, 5.01, 5)$, showing the sensitive dependence on initial conditions.

the x-coordinate of the solutions, that is the curve $(t, x(t))$, for the initial conditions $(5, 5, 5)$ and $(5, 5.01, 5)$ in order to verify the sensitive dependence on initial conditions, which is one of the main properties of strange attractors. The result is shown in figure 14(*b*). The solutions differ in their colors (or gray scale) and actually show this sensitive dependence. The y- and z-coordinates have the same behavior.

Also, in order to assure that the system presents chaotic behavior for these parameters values ($b = 0.15, \sigma = 2.3$ and $r = 7.8$) we have calculated the Lyapunov exponents, following the method presented in [15], which after 1000 iterations give

$$\lambda_1 = 0.156\,806\,8907, \qquad \lambda_2 = -1.063\,121\,4648, \qquad \lambda_3 = -4.903\,743\,7581.$$

Thus we have a positive Lyapunov exponent, indicating the chaotic behavior of the system, for these parameters values.

In figure 3(*a*) of the introduction we show the attractor obtained for $b = 0.15, \sigma = 2.3$ and $r = 200$. In figure 3(*b*) we show this attractor from another point of view: we have taken the initial conditions on the unstable manifolds of the saddle at the origin and, in this way, we can observe the spiraling behavior of the solutions around the z-axis, before tending toward the attractor. We have also calculated the Lyapunov exponents for these parameter values, which are

$$\lambda_1 = 1.663\,594\,0216, \qquad \lambda_2 = -0.476\,972\,8193, \qquad \lambda_3 = -4.855\,769\,7656,$$

confirming the chaotic behavior shown in the phase portrait.

Acknowledgments

This work was partially supported by CNPq-Brazil under the project 478544/2007-3. A preliminary version was presented at the ICMC Summer Meeting on Differential Equations: *Celebrating the* 80*th birthday of Jack K Hale*, USP–São Carlos, Brazil, January 2008.

References

[1] Carr J 1981 *Applications of Centre Manifold Theory (Applied Math. Sciencies* vol 35*)* (New York: Springer)
[2] Chow S N and Hale J K 1982 Methods of bifurcation theory *Grundlehren der Mathematischen Wissenschaften (Fundamental Principles of Mathematical Science* vol 251*)* (New York: Springer)

[3] Cima A and Llibre J 1990 Bounded polynomial vector fields *Trans. Am. Math. Soc.* **318** 557–79
[4] Doering C and Gibbon J 1995 On the shape and dimension of the Lorenz attractor *Dyn. Stab. Syst.* **10** 255–68
[5] Guckenheimer J and Holmes P 1983 *Nonlinear Oscillations, Dynamical Systems and Bifurcations of Vector Fields (Applied Math. Sciencies* vol 42*)* (New York: Springer)
[6] Hénon M 1976 A two dimensional mapping with a strange attractor *Commun. Math. Phys.* **50** 69–77
[7] Kokubu H and Roussarie R 2004 Existence of a singularly degenerate heteroclinic cycle in the Lorenz system and its dynamical consequences: Part I *J. Dyn. Differ. Equ.* **16** 513–57
[8] Llibre J, Messias M and da Silva P R 2008 On the global dynamics of the Rabinovich system *J. Phys. A: Math. Theor.* **41** 275210 (21pp)
[9] Lorenz E N 1963 Deterministic nonperiodic flow *J. Atmos. Sci.* **20** 130–41
[10] Mello L F, Messias M and Braga D C 2008 Bifurcation analysis of a new Lorenz-like chaotic system *Chaos Solitons Fractals* **37** 1244–55
[11] Pikovskii A S, Rabinovich M I and Trakhtengerts V Yu 1978 Onset of stochasticity in decay confinement of parametric instability *Sov. Phys. JETP* **47(4)** 715–9
[12] Rikitake T 1958 Oscillations of a system of disk dynamos *Proc. Camb. Phil. Soc.* **54** 89–105
[13] Sparrow C 1982 *The Lorenz Equations: Bifurcations, Chaos and Strange Attractors* (New York: Springer)
[14] Viana M 2000 What's new on Lorenz strange attractors? *Math. Intell.* **22** 6–19
[15] Wolf A, Swift J B, Swinney H L and Vastano J A 1985 Determining Lyapunov exponents from a time series *Physica* D **16** 285–317